Mühendislik Bilimleri ve Tasarım Dergisi
8(2), 625 – 634, 2020
e-ISSN: 1308-6693

Journal of Engineering Sciences and Design
DOI: 10.21923/jesd.687757

Araştırma Makalesi Research Article

INFLUENCE OF RARE EARTH SUBSTITUTION ON THE MAGNETIC PROPERTIES OF SPINEL FERRITES

Ayşe DEMİR KORKMAZ*

Department of Chemistry, Faculty of Engineering and Natural Sciences, Istanbul Medeniyet University, Uskudar, Istanbul, Turkey

Keywords

Magnetic Nanoparticles, Rare Earth Substitution, Spinel Ferrites.

Abstract

Nano-size ferrites (NSF) are magnetic nanoparticles (MNPs) which have attracted great interest in the last decades owing to their high surface area-to-volume ratio, high saturation magnetization, initial permeability, etc. Nickel-copper-zinc ferrites are especially used in multi-layer chip inductors (MLCIs) which are found in mobile phones, camcorders, notebook computers, etc. MLCIs are composed of alternating layers of silver electrodes and soft ferrites. Thus, it is important to develop magnetic characteristics in ferrites for requiring less ferrite layers and hence to obtain further miniaturized devices. The goal of our study is to investigate the effect of rare earth substitution of Ni-Cu-Zn ferrite nanoparticles. Ni-Cu-Zn NSFs substituted with rare earth metal (RE) ions Eu^{3+}, Tb^{3+}, and Dy^{3+} in varying concentrations were obtained by a sonochemical method. We investigated the crystal structure, chemical bonding, morphology and magnetic characteristics of the Ni-Cu-Zn NSFs by X-ray powder diffraction (XRD), Fourier-transform infrared spectroscopy (FT-IR), scanning electron microscopy (SEM), and vibrating sample magnetometry (VSM), respectively. The phase purity of the samples was confirmed by the XRD analysis. Stretching vibrations of spinel ferrites were verified by the FT-IR analysis. VSM results reveal that the rare earth substitution has a significant effect on the magnetic properties of the Ni-Cu-Zn NSFs.

NADİR TOPRAK KATKISININ SPİNEL FERRİTLERİN MANYETİK ÖZELLİKLERİNE ETKİSİ

Anahtar Kelimeler

Manyetik Nanoparçacıklar, Nadir Toprak Katkısı, Spinel Ferritler.

Öz

Nano boyutlu ferritler (NSF), yüksek yüzey alanı-hacim oranı, yüksek doygunluk mıknatıslanması, başlangıç manyetik geçirgenliği, vb. özellikleriyle son yıllarda büyük ilgi çeken manyetik nanoparçacıklardır (MNP). Nikel-bakır-çinko ferritler ise özellikle cep telefonlarında, video kameralarda, dizüstü bilgisayarlarda vs. bulunan çok katmanlı yonga indüktörlerinde (MLCI'lar) kullanılmaktadır. MLCI'ler alternatif gümüş elektrot ve yumuşak ferrit katmanlarından oluşur. Bu nedenle, daha az ferrit katmanı gerektiren ve dolayısıyla daha da küçültülmüş cihazların elde edilmesi için ferritlerde manyetik özelliklerin geliştirilmesi önem arz etmektedir. Çalışmamızın amacı, Ni-Cu-Zn ferrit nanoparçacıklarına nadir toprak katkısının etkilerini araştırmaktır. Çeşitli konsantrasyonlarda nadir toprak metal (RE) iyonları Eu^{3+}, Tb^{3+} ve Dy^{3+} ile katkılanmış Ni-Cu-Zn NSF'ler bir sonokimyasal yöntemle elde edildi. Ni-Cu-Zn NSF'lerin kristal yapısını, kimyasal bağını, morfolojisini ve manyetik özelliklerini sırasıyla X-ışını toz kırınımı (XRD), Fourier dönüşümü kızılötesi spektroskopisi (FT-IR), taramalı elektron mikroskobu (SEM) ve titreşimli numune manyetometrisi (VSM) ile inceledik. Numunelerin faz saflığı, XRD analizi ile doğrulandı. Spinel ferritlerin gerilme titreşimleri FT-IR analizi ile doğrulandı. VSM sonuçları, nadir toprak sübstitüsyonunun Ni-Cu-Zn NSF'lerin manyetik özellikleri üzerinde önemli bir etkisi olduğunu ortaya koymaktadır.

* İlgili yazar / Corresponding author: ayse.demir@medeniyet.edu.tr, +90-216-280-3449

Alıntı / Cite

Demir Korkmaz, A., (2020). Influence of Rare Earth Substitution on the Magnetic Properties of Spinel Ferrites, Journal of Engineering Sciences and Design, 8(2), 625-634.

Yazar Kimliği / Author ID (ORCID Number)

A. Demir Korkmaz, 0000-0002-3102-7201

Makale Süreci / Article Process

Başvuru Tarihi / Submission Date	11.02.2020
Revizyon Tarihi / Revision Date	10.06.2020
Kabul Tarihi / Accepted Date	21.06.2020
Yayım Tarihi / Published Date	25.06.2020

1. Introduction

Magnetic nanoparticles (MNPs) are nano-sized ferrites which have attracted great interest in the last decades and there is an increase in their use in various fields. Nano-sized spinel ferrites (NSFs) are a class of MNPs with superior magnetic and electrical properties such as high saturation magnetization, initial permeability, low eddy current loss, and high dielectric properties. Main uses of ferrite nanoparticles (NPs) ranging from biomedical applications to environmental and industrial applications include drug delivery, biomedical imaging (magnetic resonance imaging (MRI)), magnetic hyperthermia (Sharifi et al., 2012; Umut et al., 2019), catalysis (Dantas et al., 2013; Taghavi Fardood et al., 2017), wastewater treatment (Fu et al., 2010), capacitors (Khan et al., 2017), circulators (Harris and Sokolov, 2019), multilayer chip inductors (MLCIs) (Batoo and Ansari, 2012), etc. MLCIs, which are produced by alternating silver and Ni-Cu-Zn ferrite layers, are widely used in the telecommunication industry as well as electronics such as mobile phones, camcorders, and notebook computers. Therefore, the development of properties of Ni-Cu-Zn ferrites is essential for further miniaturizing such devices.

The magnetic, optical, and electrical properties of NSFs can be varied by introducing different cations in the spinel structure, AB_2O_4, where "A" represents tetrahedral sites and "B" represents octahedral sites. A spinel ferrite cell consists of 64 tetrahedral (Td) sites and 32 octahedral (Oh) sites occupied by 8 cations and 16 cations, respectively. Since the magnetic moment of the NSF is the difference between the magnetizations of two sub-lattices ($M=M_A-M_B$), the cation distribution within these sites can alter magnetic properties of NSF although they have the same composition and size. Therefore, many attempts have been made to obtain Ni-Cu-Zn ferrites with novel characteristics by the incorporation of different cations to the available positions in the crystal structure. The rare earth substitution in NCZF was also studied by some researchers. For example, Gabal et al. investigated the effect of lanthanum ion incorporation in NCZF prepared by using egg white. There was a rise in the size-dependent coercivity and lattice constant whereas a drop was observed for Curie temperature in La^{3+} substituted Ni-Cu-Zn ferrites (Gabal et al., 2011).

To the best of our knowledge, there are no studies comparing the effect of doping NCZF with europium, terbium, and dysprosium. Therefore, we report the preparation of $Ni_{0.4}Cu_{0.2}Zn_{0.4}RE_{0.02}Fe_{1.98}O_4$ (RE= Eu^{3+}, Tb^{3+}, Dy^{3+}) NSFs via sonochemical approach and discuss the structural and magnetic properties of RE-doped NCZF by XRD, FT-IR, and VSM measurements.

2. Experimental

The ultrasonic-induced cavitation is a sonochemical method in which a liquid is compressed and expanded suddenly by the help of ultrasound. The rapid expansion of the cavitation bubbles is followed by their collapse which is repeated for several cycles, reaching extremely high temperatures (~5000 K), high pressures (20 MPa) and a fast cooling rate (~10^6 K per second) (Goswami et al., 2013). This technique offers a shorter reaction time, the hydrolysis rate is highly enhanced, and it is possible to prepare uniformly distributed and highly pure NPs (Ahmed et al., 2015).

The synthesis of $Ni_{0.4}Cu_{0.2}Zn_{0.4}RE_{0.02}Fe_{1.98}O_4$ NSFs was achieved by a sonochemical approach. Stoichiometric amounts of metal precursors; $Ni(NO_3)_2.6H_2O$, $Cu(NO_3)_2{\cdot}6H_2O$, $Zn(NO_3)_2.6H_2O$, $Fe(NO_3)_3{\cdot}9H_2O$ and RE (III) oxide (RE= Eu^{3+}, Tb^{3+}, Dy^{3+}) were dissolved in 80 ml of deionized water + 15 ml of concentrated hydrochloric acid solution under vigorous stirring followed by adjusting the pH to 11 by using ammonia solution. The solution was exposed to ultrasonic irradiation with high-intensity (20 kHz frequency and 70 W power, (UZ SONOPULS HD 2070)) for 30 min. The powder product was obtained by washing with a mixture of DI H_2O/EtOH (50% v/v), centrifugation and drying at 100 °C for 3 h.

3. Results and Discussion

Fourier transform-infrared (FT-IR, Bruker) spectra were recorded using a spectrometer over the wavelength range 4000–400 cm^{-1}. The FT-IR spectra of $Ni_{0.4}Cu_{0.2}Zn_{0.4}RE_{0.02}Fe_{1.98}O_4$ spinel ferrites are presented in Fig. 1. Two

characteristic vibration bands of spinel ferrites are presented around 550 cm^{-1} and 400 cm^{-1} that are assigned to the vibrational bands ν_1 and ν_2 of tetrahedral (A-site) and octahedral (B-site) lattices, respectively. The wavenumbers for the ν1 band are 538, 547, and 550 cm^{-1} for Eu^{3+}, Tb^{3+}, Dy^{3+}-substituted NCZF nanoparticles, respectively. The cation distribution among A- and B-sites designates the absorption band positions for ν_1 and ν_2 vibrations (Ahmad et al., 2018). ν_1 around 550 cm^{-1} indicates the stretching band of the metal-oxygen at the tetrahedral site (M_{tetra}-O) and ν_2 band around 450 cm^{-1} is due to the metal-oxygen stretching at the octahedral site (M_{octa}-O) (Kesavamoorthi and Raja, 2017; Slimani et al., 2019). It is clear that the ν_1 vibrational band shifts to a higher frequency as the ionic radius of the substituent ion changes (Harzali et al., 2018). This is due to the distortion of the crystal structure and occupation of B-sites by the rare earth substituent ions causing a change in the bond length and hence the frequency of the absorption band (Almessiere et al., 2019a; Ansari et al., 2018).

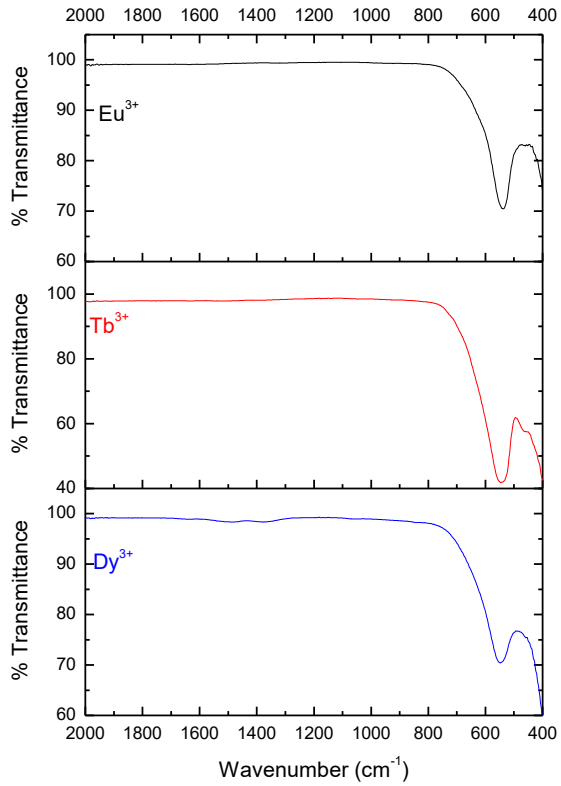

Figure 1. FT-IR spectra of $Ni_{0.4}Cu_{0.2}Zn_{0.4}RE_{0.02}Fe_{1.98}O_4$ NSFs.

3.1. XRD Analysis

Figure 2 displays the XRD patterns of $Ni_{0.4}Cu_{0.2}Zn_{0.4}RE_{0.02}Fe_{1.98}O_4$ NSFs. The diffraction peaks associated with the Bragg's reflections from (2 2 0), (3 1 1), (4 0 0), (2 2 2), (4 0 0), (4 2 2), (4 4 0) exhibit the typical crystal structure of spinel ferrites with a space group Fd-3m. We would like to note that the single phase of RE substitution in Ni-Cu-Zn ferrite is was achieved by using only the sonochemical method without further calcination. Rietveld refinement was used to calculate the structural parameters from XRD patterns with FullProf program. Average crystallites sizes were determined by Debye–Scherrer equation by using the most intense (3 1 1) peak of each sample. The refined structural parameters and crystallite sizes of the products are listed in Table 1. The lattice constant (a) slightly decreases with RE^{3+} substitution. This indicates that the larger trivalent rare earth ions were successfully incorporated into octahedral sites replacing the Fe^{3+} ions in the unit cell (Jacob et al., 2013). The crystallite sizes are found to be between 13 and 22 nm. In general, since the rare earth ions are compared to the ferric ion, the crystallite size tends to rise as the ionic radius of the RE^{3+} increases. On the other hand, the sample doped with dysprosium ion showed the minimum value in the crystallite size. This may be attributed to the formation of a secondary phase. In other samples, the crystallite size tends to decrease as the atomic number increases.

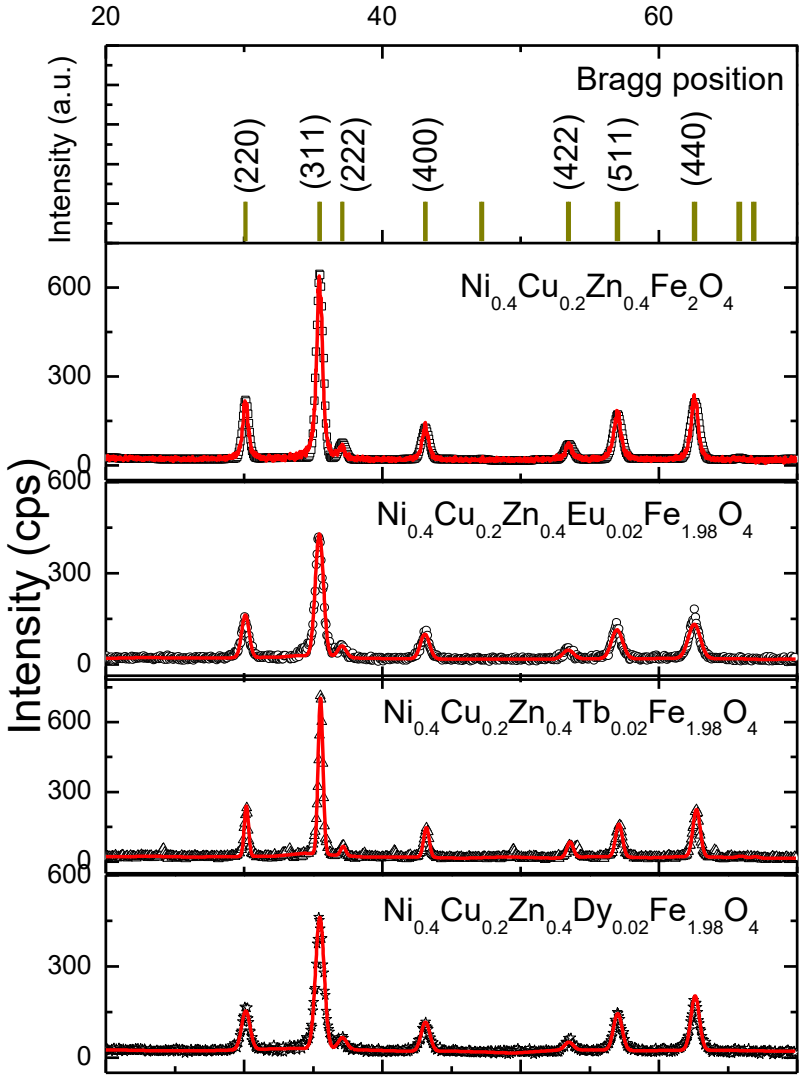

Figure 2. XRD powder patterns of $Ni_{0.4}Cu_{0.2}Zn_{0.4}Fe_2O_4$ and $Ni_{0.4}Cu_{0.2}Zn_{0.4}RE_{0.02}Fe_{1.98}O_4$ (RE=Eu^{3+}, Tb^{3+}, or Dy^{3+}) NSFs. The open symbols correspond to the experimental data and the solid red lines represent the fitted curves.

Table 1. The rare earth ion content, and refined structural parameters for $Ni_{0.4}Cu_{0.2}Zn_{0.4}Fe_2O_4$ and $Ni_{0.4}Cu_{0.2}Zn_{0.4}RE_{0.02}Fe_{1.98}O_4$ NSFs Fd-3m (No. 227) where RE is a trivalent rare earth ion (Eu^{3+}, Tb^{3+}, or Dy^{3+}) . ***a:*** Lattice constant, V: volume, D_{XRD}: crystallite size, $r_{M^{+3}}$: ionic radius of the trivalent metal ion (M).

Trivalent ion (M^{3+})	***a*** **(Å)**	***V*** **($Å^3$)**	D_{XRD} **(nm) ±0.08**	$\chi^2(chi^2)$	R_{Bragg}	$r_{M^{+3}}$ **(Å)**
Fe^{3+} (unsubstituted)	8.392(5)	591.13	17.19	1.71	5.15	0.645
Eu^{3+}	8.378(6)	588.18	18.20	1.92	3.08	0.947
Tb^{3+}	8.379(7)	588.41	22.54	1.99	2.80	0.923
Dy^{3+}	8.391(5)	590.90	13.54	1.20	1.31	0.912

3.2. TEM and SEM Analyses

The morphology, the size and the electron diffraction patterns of RE substituted Ni-Cu-Zn NSFs were investigated by a scanning electron microscope (SEM; FEI Titan ST) coupled with EDX system and transmission electron microscopy (TEM) (FEI, Morgagni 268). The TEM was used at an accelerating voltage of 80 kV. TEM images, histograms and selected area electron diffraction (SAED) patterns of $Ni_{0.4}Cu_{0.2}Zn_{0.4}RE_{0.02}Fe_{1.98}O_4$ spinel ferrites are displayed in the following figure. The particles exhibited cube-like morphology and aggregated due to their magnetic nature. The average size of the particles was estimated around 20 nm for the NSFs. The particle size estimated by TEM was in good agreement with the crystallite size calculated by the XRD analysis (Table 1). Rare earth cation substituted nickel-copper-zinc NSF exhibited isolated continuous rings in their diffraction patterns (SAED) which were recorded by TEM. The first six rings of the SAED patterns were identified as, (220), (311), (400), (422), (511) and (440). The (311) displayed the maximum diffraction intensity which is consistent with the XRD pattern as shown by Figure 3.

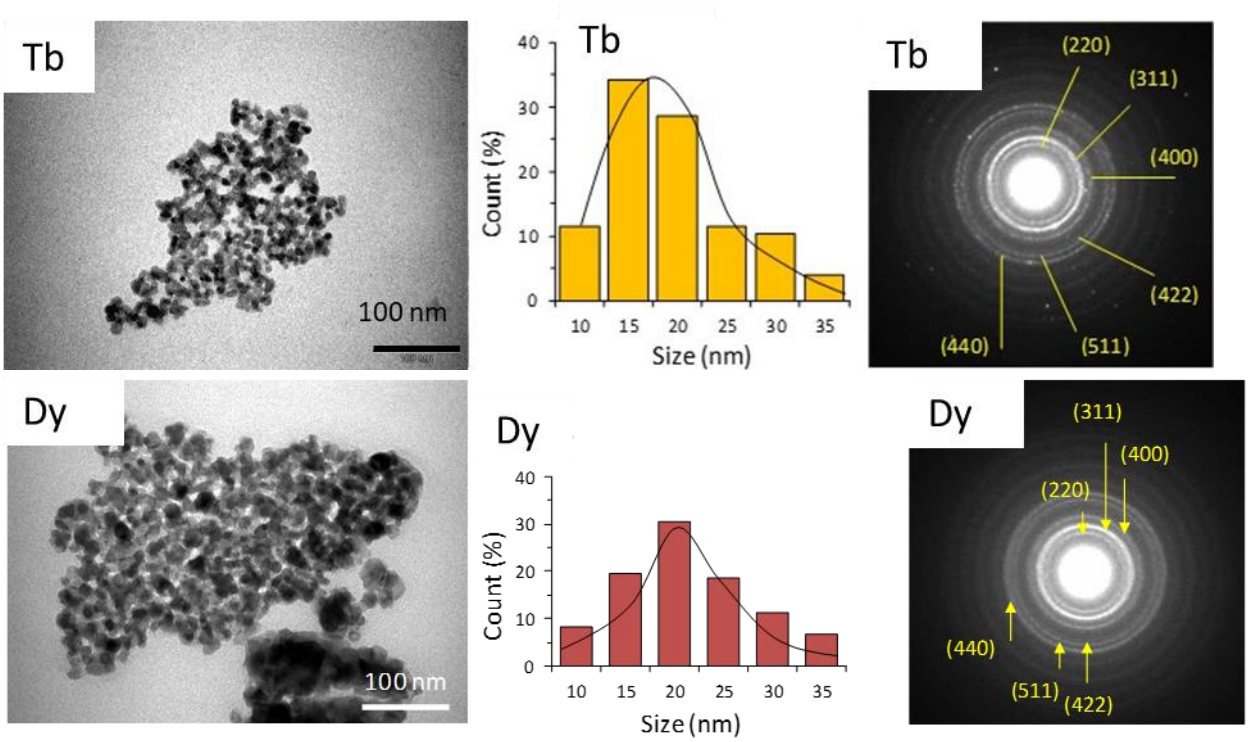

Figure 3. TEM images of Tb substituted Ni-Cu-Zn NSFs

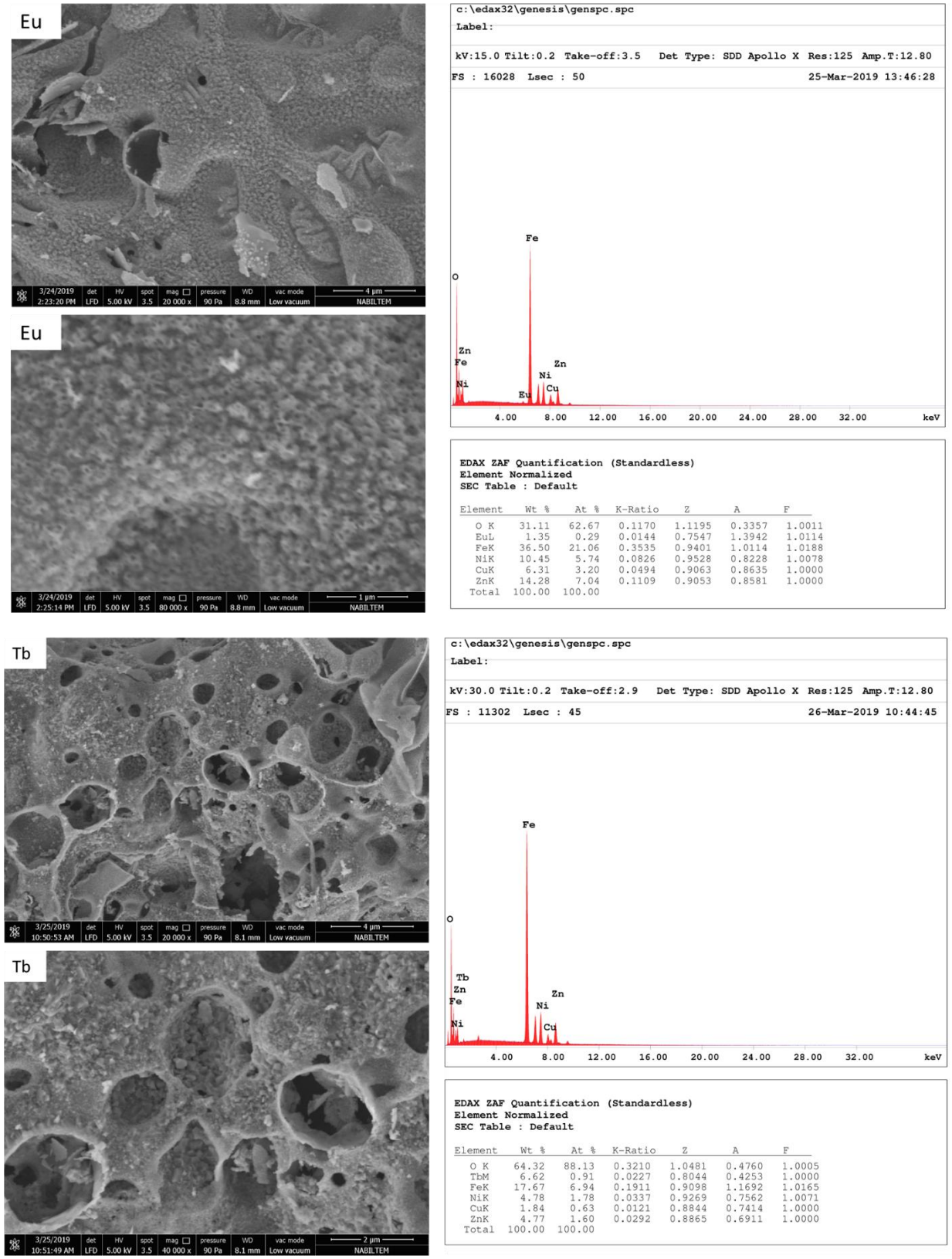

Figure 4. SEM images of $Ni_{0.4}Cu_{0.2}Zn_{0.4}RE_{0.02}Fe_{1.98}O_4$ NSFs.

3.3. VSM Analysis

A Superconducting Quantum Interference Device (SQUID) magnetometer (Quantum Design) equipped with a vibrating sample magnetometer (VSM) head was used to measure the magnetic properties of Ni-Cu-Zn ferrites. Fig. 5 illustrates the impact of the RE^{3+} substitution on the saturation magnetization (Ms), remanent magnetization (Mr) and coercivity (Hc) values of Ni-Cu-Zn ferrites. The numerical values of magnetic parameters Ms, Mr, Hc, S (remanence squareness: S = Mr/Ms), and μ_B (experimental magnetic moment) were listed in **Table 2**. All ferrites

exhibit an S shaped hysteresis curve with no coercivity at room temperature (RT), hence superparamagnetic behavior, and very low coercivities at low temperature (10 K) which indicate their soft magnetic characteristics. The coercivity values follow a similar trend with crystallite sizes as expected. In addition, the unsubstituted NCZF nanoparticles display Ms values of 42.06 emu/g and 68.77 emu/g at RT and 10 K, respectively. These values are lower when compared to their bulk inverse counterpart, which can be assigned due to the presence of much smaller ferrite crystallites in the sample (Liang-Qiu et al., 2011). The decrease in the Ms value of the NCZF NPs can be explained by the core-shell model. The core has spins that are aligned magnetically whereas the shell, surface of the nanoparticle displays a spin glass-like state owing to the disrupted exchange interactions (Priyadharsini et al., 2009). The surface-to-volume ratio in nanoparticles is considerably larger and therefore, the larger surface has an impact on the magnetization by spin disordering. In general, Ms and Mr values and coercivities of RE^{3+} substituted NCZF nanoparticles are smaller than that $Ni_{0.4}Cu_{0.2}Zn_{0.4}Fe_2O_4$ nanoparticles and follow a decreasing trend with the increasing atomic number of dopants at both RT and low temperature. In the spinel ferrite crystal structure, there are two types of superexchange interactions: inter-sublattice between A and B sites and intra-sublattice between A-A sites as well as between B-B sites. According to Néel's model, the inter-sublattice interactions are considerably stronger than the intra-sublattice interactions (Néel, 1948). In the undoped ferrite, the main contribution to the magnetization comes from highly magnetic ferric ions (5 μ_B) that are present in the B sites (Kadam et al., 2012). Upon doping, the occupancy of the octahedral sites (B) are preferred by the larger rare earth ions and therefore there will be less number of Fe^{3+} ions to occupy B sites. This will result in weaker B-B interactions and hence A-B interactions and consequently the magnetic moment will be lowered owing to the replacement of ferric ions with non-magnetic rare earth ions (Dasan et al., 2017). The antiferromagnetic coupling between A and B sites arises and spinel lattice is distorted due to the substitution of $Fe^{3+}$with RE^{3+} are other factors which contribute to the drop in the magnetization.

The experimental magnetic moment, μ_B *(obs),* was calculated by the following equation $\mu_B(obs) = (Mw \times Ms) / 5585$ where Mw is the molar mass of the compound and Ms stands for saturation magnetization. μ_B values calculated are between 2.434 and 2.820 which are lower than that of the undoped NSF at RT. The Bohr magneton decreases by increasing molecular weight and is the minimum for the Dy^{3+} substituted NCZF. This might be due to the weakening of inter-sublattice (A-B) superexchange interactions (Almessiere et al., 2019c). The remanenece squareness can give information about the grain variation. Values for remanence squarenesss at both temperatures were found to be lower than 0.5 which indicate the synthesized nanoparticles have a single domain nature with uniaxial anisotropy and the easy axis being randomly oriented according to Stoner-Wohlfarth theory (Caruntu et al., 2007; Saura-Múzquiz et al., 2016; Stoner and Wohlfarth, 1948). In addition, remanence squareness values lower than 0.5 indicate a strong spin-disordering exists on the surface (Almessiere et al., 2019b; Sadaqat et al., 2019).

Table 2. The deduced magnetic parameters of the $Cu_{0.4}Ni_{0.2}Zn_{0.4}$ $RE_{0.02}Fe_{1.98}O_4$ NSFs at 10 K (M_{max},20: max magnetization at 20 kOe, Ms: saturation magnetization, Mr: remanence magnetization, S: remanence squareness, Hc: coercivity and nB: magnetic moment))

Compound		**10 K**				**300 K**				
	MW (g/mol)	***Ms (emu/g)***	***Hc (kOe)***	***Mr (emu/g)***	***S***	$\mu_{f.u.}$ (μ_B)	***Ms (emu/g)***	***Hc (kOe)***	***Mr (emu/g)***	***S***
$Cu_{0.4}Ni_{0.2}Zn_{0.4}Fe_2O_4$	238.032	68.77	0.17	17.18	0.250	2.931	42.06	0.046	4.15	0.0985
$Cu_{0.4}Ni_{0.2}Zn_{0.4}Eu_{0.02}Fe_{1.98}O_4$	239.955	65.63	0.18	15.51	0.236	2.820	41.35	0.050	5.02	0.123
$Cu_{0.4}Ni_{0.2}Zn_{0.4}Tb_{0.02}Fe_{1.98}O_4$	240.094	61.04	0.073	9.34	0.153	2.624	40.65	0.049	4.61	0.113
$Cu_{0.4}Ni_{0.2}Zn_{0.4}Dy_{0.02}Fe_{1.98}O_4$	240.166	56.60	0.11	7.63	0.134	2.434	25.23	0.001	0.46	0.309

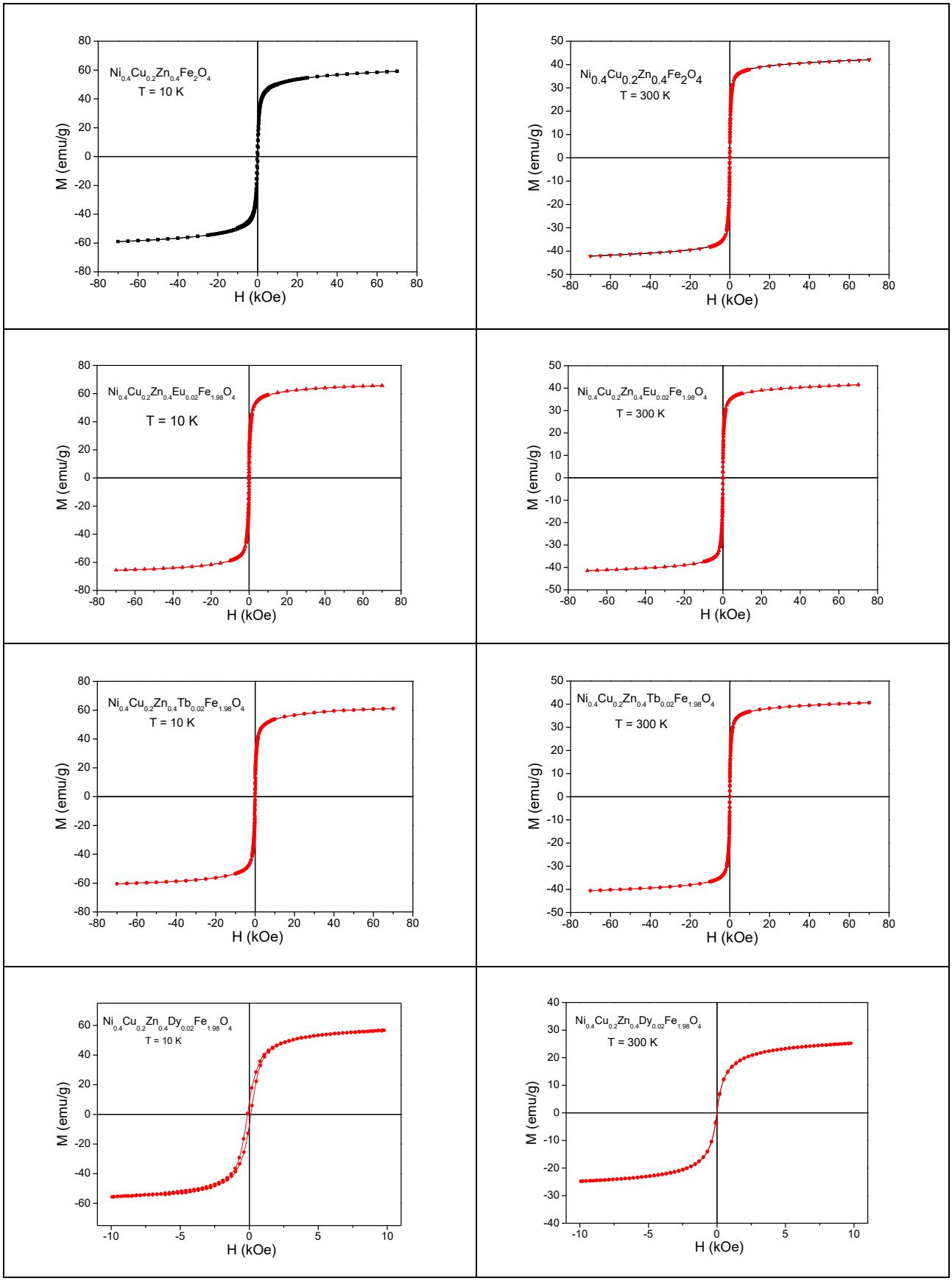

Figure 5. Magnetization (M) vs. applied field (H) of ±10 kOe, curves, M(H) for undoped and doped $Ni_{0.4}Cu_{0.2}Zn_{0.4}RE_{0.02}Fe_{1.98}O_4$ NSFs; Left: at 10 K, and. Right: at RT.

4. Conclusion

In this study, nano-sized Ni-Cu-Zn ferrites substituted with rare earth ions Eu^{3+}, Tb^{3+}, and Dy^{3+} in were prepared by a sonochemical method. The FT-IR spectra depicted the vibrational bands of spinel ferrites. The XRD results revealed that the products showed a spinel ferrite structure with phase homogeneity. In general the crystallite sizes (13-22 nm) increased with the rise of the ionic radius of the dopant ions. In addition, there was a slight drop in the lattice parameter (a) with RE^{3+} substitution, which confirmed the incorporation of the rare earth ions. TEM and SEM analyses verified the cube-like nanoparticles with sizes (around 20 nm) similar to the crystallite sizes calculated from XRD results and diffraction patterns of the particles. The magnetization studies conducted by VSM analysis displayed the nanoparticles exhibited superparamagnetic behavior at room temperature and very low coercivity values at 10 K indicating their soft magnetic characteristics. The coercivity values were found to be in parallel with crystallite sizes. The octahedral site preference of the rare earth ions caused a decrease in the saturation magnetization values. A drop in the saturation magnetization values was observed with a decrease in the ionic size of the dopant ions.

Conflict of Interest

No conflict of interest was declared by the author.

References

Ahmad, S.I., Ansari, S.A., Ravi Kumar, D., 2018. Structural, morphological, magnetic properties and cation distribution of Ce and Sm co-substituted nano crystalline cobalt ferrite. Materials Chemistry and Physics, 208, 248-257.

Ahmed, M., Ramulu Torati, S., Parvatheeswara Rao, B., Abdel Hamed, M., Kim, C. 2015. Size controlled sonochemical synthesis of highly crystalline superparamagnetic Mn–Zn ferrite nanoparticles in aqueous medium.

Almessiere, M.A., Demir Korkmaz, A., Slimani, Y., Nawaz, M., Ali, S., Baykal, A., 2019a. Magneto-optical properties of rare earth metals substituted Co-Zn spinel nanoferrites. Ceramics International, 45, 3449-3458.

Almessiere, M.A., Slimani, Y., Güner, S., Baykal, A., Ercan, I., 2019b. Effect of dysprosium substitution on magnetic and structural properties of $NiFe_2O_4$ nanoparticles. Journal of Rare Earths, 37, 871-878.

Almessiere, M.A., Slimani, Y., Güner, S., Nawaz, M., Baykal, A., Aldakheel, F., Akhtar, S., Ercan, I., Belenli, İ., Ozçelik, B., 2019c. Magnetic and structural characterization of Nb^{3+}-substituted $CoFe_2O_4$ nanoparticles. Ceramics International, 45, 8222-8232.

Ansari, M.M.N., Khan, S., Ahmad, N., 2018. Effect of R^{3+} (R = Pr, Nd, Eu and Gd) substitution on the structural, electrical, magnetic and optical properties of Mn-ferrite nanoparticles. Journal of Magnetism and Magnetic Materials, 465, 81-87.

Batoo, K.M., Ansari, M.S., 2012. Low temperature-fired Ni-Cu-Zn ferrite nanoparticles through auto-combustion method for multilayer chip inductor applications. Nanoscale Research Letters, 7, 112.

Caruntu, D., Caruntu, G., O'Connor, C.J., 2007. Magnetic properties of variable-sized Fe_3O_4 nanoparticles synthesized from non-aqueous homogeneous solutions of polyols. Journal of Physics D: Applied Physics, 40, 5801.

Dantas, J., Santos, J.R.D., Cunha, R.B.L., Kiminami, R.H.G., Costa, A.C.F., 2013. Use of Ni-Zn ferrites doped with Cu as catalyst in the transesterification of soybean oil to methyl esters. Materials Research, 16, 625-627.

Dasan, Y.K., Guan, B.H., Zahari, M.H., Chuan, L.K., 2017. Influence of La^{3+} Substitution on Structure, Morphology and Magnetic Properties of Nanocrystalline Ni-Zn Ferrite. PLOS ONE, 12, e0170075.

Fu, Y.-P., Chang, W.-K., Wang, H.-C., Liu, C.-W., Lin, C.-H., 2010. Synthesis and characterization of anatase TiO_2 nanolayer coating on Ni–Cu–Zn ferrite powders for magnetic photocatalyst. Journal of Materials Research, 25, 134-140.

Gabal, M.A., Asiri, A.M., AlAngari, Y.M., 2011. On the structural and magnetic properties of La-substituted NiCuZn ferrites prepared using egg-white. Ceramics International, 37, 2625-2630.

Goswami, P.P., Choudhury, H.A., Chakma, S., Moholkar, V.S., 2013. Sonochemical Synthesis and Characterization of Manganese Ferrite Nanoparticles. Industrial & Engineering Chemistry Research, 52, 17848-17855.

Harris, V.G., Sokolov, A.S., 2019. The Self-Biased Circulator: Ferrite Materials Design and Process Considerations. Journal of Superconductivity and Novel Magnetism, 32, 97-108.

Harzali, H., Marzouki, A., Saida, F., Megriche, A., Mgaidi, A., 2018. Structural, magnetic and optical properties of nanosized $Ni_{0.4}Cu_{0.2}Zn_{0.4}R_{0.05}Fe_{1.95}O_4$ (R = Eu^{3+}, Sm^{3+}, Gd^{3+} and Pr^{3+}) ferrites synthesized by co-precipitation method with ultrasound irradiation. Journal of Magnetism and Magnetic Materials, 460, 89-94.

Jacob, B.P., Thankachan, S., Xavier, S., Mohammed, E.M., 2013. Effect of Tb^{3+} substitution on structural, electrical and magnetic properties of sol–gel synthesized nanocrystalline nickel ferrite. Journal of Alloys and Compounds, 578, 314-319.

Kadam, R.H., Karim, A., Kadam, A.B., Gaikwad, A.S., Shirsath, S.E., 2012. Influence of Cr^{3+} substitution on the electrical and magnetic properties of $Ni_{0.4}Cu_{0.4}Zn_{0.2}Fe_2O_4$ nanoparticles. International Nano Letters, 2, 28.

Kesavamoorthi, R., Raja, C.R., 2017. Substitution Effects on Rare-Earth Ions-Doped Nickel-Zinc Ferrite Nanoparticles. Journal of Superconductivity and Novel Magnetism, 30, 1207-1212.

Khan, M.Z., Gul, I.H., Anwar, H., Ameer, S., Khan, A.N., Khurram, A.A., Nadeem, K., Mumtaz, M., 2017. Massive dielectric properties enhancement of MWCNTs/$CoFe_2O_4$ nanohybrid for super capacitor applications. Journal of Magnetism and Magnetic Materials, 424, 382-387.

Liang-Qiu, G., Guo-Jian, Y., Ying, W., Fu-Lin, W., 2011. Study of NiCuZn ferrite powders and films prepared by sol—gel method. Chinese Physics B, 20, 027503.

Néel, M.L., 1948. Propriétés magnétiques des ferrites ; ferrimagnétisme et antiferromagnétisme. Annales de Physique, 12, 137-198.

Priyadharsini, P., Pradeep, A., Chandrasekaran, G., 2009. Novel combustion route of synthesis and characterization of nanocrystalline mixed ferrites of Ni–Zn. Journal of Magnetism and Magnetic Materials, 321, 1898-1903.

Sadaqat, A., Almessiere, M., Slimani, Y., Guner, S., Sertkol, M., Albetran, H., Baykal, A., Shirsath, S.E., Ozcelik, B., Ercan, I., 2019. Structural, optical and magnetic properties of Tb^{3+} substituted Co nanoferrites prepared via sonochemical approach. Ceramics International, 45, 22538-22546.

Saura-Múzquiz, M., Granados-Miralles, C., Stingaciu, M., Bøjesen, E.D., Li, Q., Song, J., Dong, M., Eikeland, E., Christensen, M., 2016. Improved performance of $SrFe_{12}O_{19}$ bulk magnets through bottom-up nanostructuring. Nanoscale, 8, 2857-2866.

Sharifi, I., Shokrollahi, H., Amiri, S., 2012. Ferrite-based magnetic nanofluids used in hyperthermia applications. Journal of magnetism and magnetic materials, 324, 903-915.

Slimani, Y., Almessiere, M.A., Nawaz, M., Baykal, A., Akhtar, S., Ercan, I., Belenli, I., 2019. Effect of bimetallic (Ca, Mg) substitution on magneto-optical properties of $NiFe_2O_4$ nanoparticles. Ceramics International, 45, 6021-6029.

Stoner, E.C., Wohlfarth, E.P., 1948. A mechanism of magnetic hysteresis in heterogeneous alloys. Philosophical Transactions of the Royal Society of London. Series A, Mathematical and Physical Sciences, 240, 599-642.

Taghavi Fardood, S., Ramazani, A., Golfar, Z., Joo, S.W., 2017. Green synthesis of Ni-Cu-Zn ferrite nanoparticles using tragacanth gum and their use as an efficient catalyst for the synthesis of polyhydroquinoline derivatives. Applied Organometallic Chemistry, 31, e3823.

Umut, E., Coşkun, M., Pineider, F., Berti, D., Güngüneş, H., 2019. Nickel ferrite nanoparticles for simultaneous use in magnetic resonance imaging and magnetic fluid hyperthermia. J Colloid Interface Sci, 550, 199-209.